

Optimized Vessel Segmentation: A Structure-Agnostic Approach with Small Vessel Enhancement and Morphological Correction

Dongning Song, Weijian Huang, Jiarun Liu, Md Jahidul Islam, Hao Yang and Shanshan Wang*

Abstract—Accurate segmentation of blood vessels is essential for various clinical assessments and postoperative analyses. However, the inherent challenges of vascular imaging—such as sparsity, fine granularity, low contrast, data distribution variability, and the critical need for preserving topological structure—make generalized vessel segmentation particularly complex. While specialized segmentation methods have been developed for specific anatomical regions, their over-reliance on tailored models hinders broader applicability and generalization. General-purpose segmentation models introduced in medical imaging often fail to address critical vascular characteristics, including the connectivity of segmentation results. To overcome these limitations, we propose an optimized vessel segmentation framework: a structure-agnostic approach incorporating small vessel enhancement and morphological correction for multi-modality vessel segmentation. To train and validate this framework, we compiled a comprehensive multi-modality dataset spanning 17 datasets and benchmarked our model against six SAM-based methods and 17 expert models. The results demonstrate that our approach achieves superior segmentation accuracy, generalization, and a 34.6% improvement in connectivity, underscoring its clinical potential. An ablation study further validates the effectiveness of the proposed improvements. We will release the code and dataset at github.com following the publication of this work.

Index Terms—Vessel segmentation, segment anything, medical image analysis.

I. INTRODUCTION

VESSEL segmentation plays a crucial role in analyzing various related diseases [1]. However, manual observation by doctors is often time-consuming, tedious, and requires a high level of expertise [2]. Therefore, developing an automatic, accurate, and highly generalizable vessel segmentation method using computer technology holds significant promise for clinical applications.

In medical image analysis, many pioneers have developed automated vessel segmentation models to reduce clinical workloads and enhance diagnostic efficiency. Early research primarily focused on traditional machine learning algorithms,

This research was partly supported by the National Natural Science Foundation of China (No. 62222118, No. U22A2040), Shenzhen Science and Technology Program (No. RYX20210706092104034, No. JCYJ20220531100213029), Shenzhen Medical Research Fund (No. B2402047), the Major Key Project of PCL under Grant PCL2024A06, Key Laboratory for Magnetic Resonance and Multimodality Imaging of Guangdong Province (No. 2023B1212060052), and Youth Innovation Promotion Association CAS.

Thanks, D. Song, W. Huang, J. Liu, M. J. Islam, H. Yang, and S. Wang are with the Paul C. Lauterbur Research Center for Biomedical Imaging, Shenzhen Institutes of Advanced Technology, Chinese Academy of Sciences, Shenzhen 518055, China (e-mail: ss.wang@siat.ac.cn).

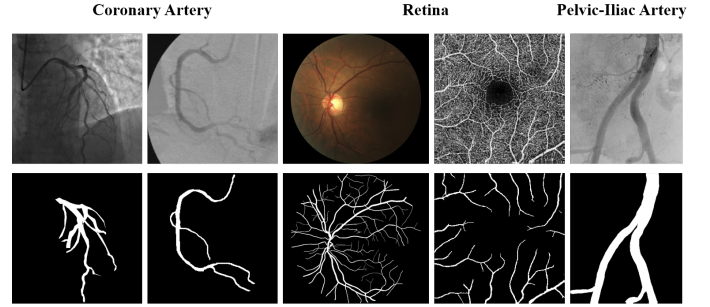


Fig. 1. The distribution of vascular imaging data shows significant variation across different anatomical regions and acquisition protocols, posing challenges for the generalization of task-specific expert models.

in which vessels were identified and segmented using manually extracted features. For instance, Chaudhuri *et al.* [3] proposed a method utilizing a two-dimensional matched filter for retinal vessel detection, while Hoover *et al.* [4] employed matched filters for vessel segmentation. Recently, with the advancement of deep learning—particularly the development of attention mechanisms [5] and convolutional neural networks (CNNs) [6]—automated vessel segmentation has seen substantial improvements in both efficiency and accuracy. These innovations have further strengthened the role of computer-assisted medical analysis. Building on these advancements, recent progress in artificial intelligence has led to the emergence of large-scale foundational models [7], ushering in a new era of AI with remarkable zero-shot and few-shot generalization capabilities across various downstream tasks. Among these foundational models, the Segment Anything Model (SAM) [8] has gained attention as a universal model for visual segmentation. Its robust cross-object segmentation abilities and impressive zero-shot generalization have made SAM particularly promising in medical imaging applications, demonstrating significant potential in addressing challenges traditionally faced by task-specific segmentation models [9].

However, accurate, generalized, and topology-preserving vessel segmentation remains a challenging task. While blood vessels are inherently difficult to segment due to their fine granularity, sparsity, low contrast, and variable shapes, the key challenges lie in the model’s generalization across diverse datasets and its ability to preserve topological integrity during segmentation. First, as shown in fig. 1, significant variations in vascular imaging data across different anatomical locations and acquisition protocols [10] create substantial difficulties

for model generalization. Models trained on a single dataset or modality often fail to perform well when applied to new datasets, leading to resource inefficiency, redundant model development, and deployment obstacles. The ability to generalize across such diverse data distributions is critical to ensuring the practical applicability of vessel segmentation models in real-world clinical settings. Second, unlike other segmentation tasks, vessel segmentation requires a strong focus on preserving the topological structure of the vascular network. Inaccuracies such as discontinuities, fractures, or merging of parallel vessels can severely impact the clinical utility of the segmentation [11]. For example, errors at bifurcations or crossings in retinal vessels, which are often tiny and curved, can lead to incorrect analyses, potentially affecting surgical planning, lesion diagnosis, and interventional treatments [12]. Moreover, segmentation algorithms optimized for overlap scores tend to overlook small or fragile vascular structures, which can result in fragmented segmentation, especially problematic in clinical applications where accuracy is paramount. Thus, to achieve accurate, generalized, and topology-preserving vessel segmentation, models must address both the challenges of generalization across varying data distributions and the critical need for topological integrity in the segmentation process.

In this paper, we propose OVS-Net, a structure-agnostic approach designed for optimized vessel segmentation. To adapt the universal segmentation model for vessel segmentation, we developed a dual-branch feature extraction module, consisting of a macro vessel extraction module and a micro vessel enhancement module, and modified the decoder to improve vessel segmentation mask prediction. Specifically, the original encoder is tasked with extracting features from macro and main vessels, while the micro-vessel enhancement module amplifies features of smaller vessels. Additionally, lower-level features of the micro-vessels are integrated into the decoder to further exploit multi-scale vascular information. Furthermore, we designed a topology repair network to address disconnected vessels resulting from the segmentation process, making the overall architecture more suitable for clinical use. To train and evaluate our model, we compiled a large vascular dataset incorporating 17 datasets, extensive experiments demonstrated the effectiveness of our method. The key contributions of this paper are summarized as follows:

- 1) Development of OVS-Net: We introduced OVS-Net, a structure-agnostic segmentation framework designed for optimized vessel segmentation across diverse modalities and anatomical structures.
- 2) Comprehensive Dataset Collection: We curated 17 datasets to train and evaluate OVS-Net, providing data splits and download instructions on GitHub to promote transparency and reproducibility.
- 3) Innovative Module Design: Developed a macro vessel extraction-micro vessel enhancement dual-branch module to effectively capture small vessel structures. Integrated feature connections into the mask decoder, adapting universal segmentation methods specifically for vessel segmentation tasks. Designed a post-processing network to improve segmentation connectivity and en-

hance clinical applicability.

- 4) Extensive Experimental Validation: Conducted rigorous testing across 17 datasets, demonstrating OVS-Net's superior segmentation accuracy, generalization capabilities, and a 34.6% improvement in connectivity, showcasing its potential for clinical applications.

II. RELATED WORK

A. Vessel Segmentation Methods

Accurate segmentation of blood vessels is crucial for evaluating various disorders, particularly cardiovascular diseases, as well as for surgical planning and monitoring treatment progress. This process plays a vital role in clinical analysis. With advancements in deep learning, there has been growing recognition of the importance of integrating multi-scale information in vessel segmentation. As a result, numerous methods have been proposed for the automated segmentation of blood vessels.

In fundus retinal vessel segmentation, Wu *et al.* [13] proposed SCS-Net, which combines a semantic context aggregation module to enhance multi-scale information extraction and an adaptive feature fusion module to improve integration across adjacent layers. Jiang *et al.* [14] introduced Covi-Net, which integrates a Local and Global Feature Aggregation (LGFA) module, preserving the ability to process local information while facilitating the processing of distant global information. Kang *et al.* [15] proposed CFI-Net, a model that employs joint refinement downsampling to mitigate spatial information loss caused by downsampling, preserving the details and edge features of retinal vessels. In OCTA image segmentation, Ning *et al.* [16] proposed FR-Net, an efficient and accurate network that leverages a modified Recurrent ConvNeXt Block within a full-resolution convolutional framework. This network reduces parameters and accelerates inference speed. Ma *et al.* [17] addressed data imbalance in the OCTA dataset by proposing CoSNet, which utilizes global contrastive learning to allow the network to learn both local and global features. Additionally, Ma *et al.* [18] proposed OCTA-Net, which uses a coarse segmentation module to generate preliminary vessel confidence maps and a fine segmentation module to refine the contours and shapes of retinal microvessels. In coronary artery segmentation, Chang *et al.* [19] proposed SE-RegUNet, which combines a RegNet encoder with squeeze-and-excitation blocks to enhance feature extraction. Liu *et al.* [20] introduced FR-UNet, which uses a multi-resolution convolutional mechanism to expand both horizontally and vertically while maintaining full image resolution. Despite their contributions, the aforementioned methods are specialized models tailored to specific datasets, and their performance may significantly degrade when applied to new data or different scenarios, which hinder deployment and limit their generalization to other vascular regions.

B. Segment Anything Models

In recent years, visual foundational models tailored for specific segmentation tasks have gained increasing attention. The Segment Anything Model (SAM) [8], the first large

foundational model designed for segmentation, has not only demonstrated outstanding performance on natural images but also shown remarkable promise for generalization in medical image analysis. Huang *et al.* [9] evaluated SAM’s applicability in medical contexts, highlighting its significant potential in medical image segmentation. Ma *et al.* [21] proposed MedSAM, trained on a large dataset of over 1 million images across 11 imaging modalities, which outperformed U-Net expert models in segmentation tasks. SAM-med2d [22] and Medical SAM Adapter [23] introduced Adapter modules, while SAMed [24] utilized LoRA for efficient fine-tuning, achieving high performance across multiple medical image segmentation tasks. Chai *et al.* [25] developed a staged fine-tuning approach that integrates a complementary CNN encoder with the SAM architecture, focusing on fine-tuning only the CNN and SAM decoder to minimize computational resources and training time. Similarly, Lin *et al.* [26] proposed SAMUS, which integrates a parallel CNN branch to inject local features into the ViT encoder, with position and feature adapters to modify SAM for clinically friendly deployment on smaller input sizes. Qin *et al.* [27] introduced DB-SAM, combining a ViT branch and a convolution branch to bridge the domain gap between natural images and 2D/3D medical images.

Despite the impressive performance of SAM in general medical segmentation, its results in vascular imaging may not be as favorable. While SAM’s ViT-based image encoder excels at global context modeling and provides a larger receptive field, it tends to capture global and low-frequency information [28]. However, vessel images are characterized by fine-grained and sparse features, with numerous micro-vessels, posing a challenge for the ViT encoder, which is less effective at capturing detailed, high-frequency information. While fine-tuning SAM on vascular data can improve performance, it often results in the loss of small vessels and fragmentation.

To address these issues, Ke *et al.* [28] proposed HQ-SAM, which introduced a learnable high-quality output token into the SAM mask decoder to predict more accurate masks. They also fused mask encoding with early and final ViT features to enhance mask details. Yuan *et al.* [29] proposed RWKV-SAM, which combined convolution and RWKV operations with an efficient decoder and multi-scale tokens to generate high-quality segmentation masks. Despite these advancements, there is still no universal segmentation model specifically designed for vascular imaging. Furthermore, existing methods often overlook topological preservation in segmentation, limiting their effectiveness in universal vessel segmentation.

C. Topology Correction-Based Post-Processing Method

The connectivity of vascular structure segmentation holds significant clinical value in medical applications [12], [30]. Although it may not lead to a large improvement in overlap metrics such as the Dice score, it considerably boosts the practical interpretability and visual quality for physicians [11]. The issue of connectivity differs from general segmentation tasks, since the area prone to disconnection normally arise in thin microstructure, which is less highlighted in overlap-oriented optimizations [31]. As a consequence, common segmentation

optimization algorithms mostly fail to handle this, resulting in vessel discontinuities. To address this challenge, various research has proposed additional post-processing strategies that enhance segmentation connectivity.

Teichmann *et al.* proposed ConvCRF [32], which combines the structured modeling capabilities of Conditional Random Fields (CRF) with the feature extraction power of Convolutional Neural Networks (CNN) to effectively execute CRF on GPUs. Jha *et al.* introduced a dual UNet architecture [33], where two UNets are employed to generate coarse and refined segmentation results, respectively. Yeet *et al.* designed VSR-Net [34], which utilizes a Curve Clustering Module (CCM) to build fragmented clusters, then patches the broken segments with a specially designed Curve Merging Module (CMM). Wang *et al.* introduced SegRefiner [35], which incorporates a diffusion model to refine coarse masks by employing a discrete diffusion process.

III. METHOD

A. Overview

To adapt the universal segmentation model for vessel segmentation while maintaining its strong generalization capability and leveraging its pre-trained weights, we developed OVS-Net. The model consists of five main modules: the macro vessel extraction module, the micro vessel enhancement module, the mask prediction module, the prompt encoder module, and the morphological correction-based post-processing network module. The overall architecture is illustrated in Figure 2. The macro vessel extraction module retains the ViT image encoder backbone from SAM and introduces feature and spatial adapters to better align the model with vascular characteristics. The micro vessel enhancement module uses a convolutional network based on ConvNext and FPN to improve the extraction of small vessel features. We kept the original design of the prompt encoder. The mask prediction module builds on the SAM mask decoder backbone, with enhanced feature connections to improve segmentation accuracy. Finally, the morphological correction-based post-processing network module is based on a simple U-Net architecture, designed to refine the pre-segmentation mask, ensuring improved connectivity and structural integrity in the final output. For vascular images, the network performs two segmentation predictions. The primary segmentation network, comprising the macro vessel extraction module, micro vessel enhancement module, prompt encoder module, and mask prediction module, generates the initial vessel segmentation mask. The post-processing network then generates a secondary prediction to repair disconnected vessels while preserving the intended separations. A detailed description of the implementation of each module is provided in the following sections.

B. Macro Vessel Extraction Module

The original SAM architecture consists of three main components: the image encoder, the prompt encoder, and the mask decoder. The image encoder is based on the ViT network, pre-trained with Masked Autoencoders (MAE) [36], and is responsible for encoding the input image. The encoded image

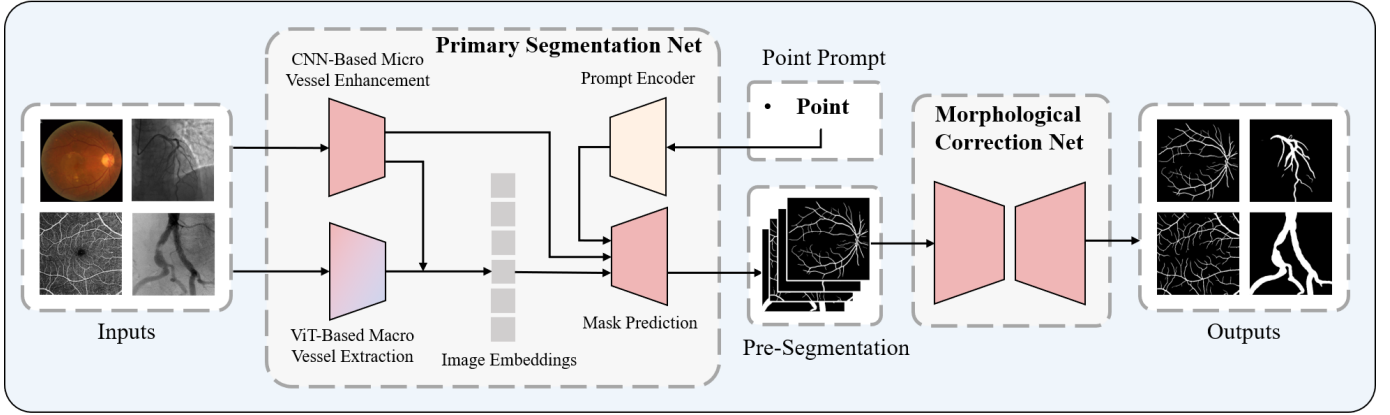


Fig. 2. Framework diagram of OVS-Net, which comprises five main modules: the ViT-based macro vessel extraction module, the CNN-based micro vessel enhancement module, the mask prediction module, the prompt encoder and the morphological correction-based post-processing network.

is then combined with the prompt encoding from the prompt encoder before being passed to the mask decoder. Due to the superior receptive field of the ViT encoder, we retain the original SAM ViT encoder architecture, using it as the backbone for the macro vessel extraction module.

To enable more efficient fine-tuning, we introduce an Adapter into each ViT block while freezing the parameters of the original ViT encoder during training. The Adapter consists of two components: a feature adapter and a spatial adapter, with the latter augmented by residual connections to enhance performance. Specifically, the spatial adapter is applied with skip connections after the Multi-Head Self-Attention (MHSA) layer, followed by the addition of the feature adapter after LayerNorm. This structure allows for effective feature extraction while preserving spatial information, enabling the model to adapt to the vessel segmentation task and ensuring successful macro-vessel extraction, all while keeping the ViT encoder parameters frozen. The procedures for the spatial adapter and feature adapter are outlined as follows:

$$S_A(X) = X + W_2 \cdot G(W_1 \cdot X) \quad (1)$$

$$F_A(X) = W_2 \cdot G(W_1 \cdot X) \quad (2)$$

where $W_1 \in \mathbb{R}^{D \times \frac{D}{4}}$, $W_2 \in \mathbb{R}^{\frac{D}{4} \times D}$, and G denotes the GELU function.

With this design, we can fine-tune the model more efficiently while keeping the ViT encoder parameters frozen. Additionally, to improve the model's ability to extracting micro-vessel features, we incorporated a convolution-based micro vessel enhancement module.

C. Micro Vessel Enhancement Module

The micro vessel enhancement module is built on ConvNext-tiny [37] and consists of four ConvNext stages. To enhance its ability to capture micro-vessel features, we integrate Convolutional Block Attention Module (CBAM) blocks into each ConvNext stage. This integration enriches feature representation while suppressing background noise and interference from surrounding tissues, especially in areas

requiring focused attention. The four ConvNext stages contain 3, 3, 9, and 3 ConvNext blocks, respectively, resulting in feature dimensions of 96, 192, 384, and 768.

To further refine the extracted features, we introduce a feature pyramid after the ConvNext stages. This addition enhances the multi-scale representation of the convolutional features, improving their compatibility with the global features from the macro vessel extraction module. We use cross-attention to fuse the global and micro-vessel features. The micro vessel enhancement module adapts its attention based on the macro vessels, allowing it to focus more effectively on important features. Likewise, the global features extracted by the macro vessel extraction module are integrated with micro-vessel features to capture finer vascular details. This synergy enables the model to more accurately extract information from vessels of varying sizes.

D. Mask Prediction Module

The mask prediction module is based on the original mask decoder from SAM, which consists of a lightweight transformer layer and a segmentation head for mask prediction. Although this step is fundamental to segmentation, we aim to improve accuracy by incorporating ideas from prior work [28], which emphasize the need for both rich global semantic context and fine local boundary details. To better integrate global and local features, we introduce a fusion of high-level and low-level features within the mask decoder. Specifically, we combine the shallow features from the first ConvNext stage with the mask features produced by the two-way transformer in the mask decoder. The shallow features capture more local information and edge details, which are crucial for accurately delineating vessel boundaries. By fusing these shallow features with the global mask features, we inject local details into the segmentation process, thereby improving the overall accuracy of the mask prediction. This fusion approach allows the model to better preserve fine vascular details, ensuring that small vessels and complex structures are accurately segmented. The combination of high-level and low-level features helps the model achieve a more comprehensive understanding of the

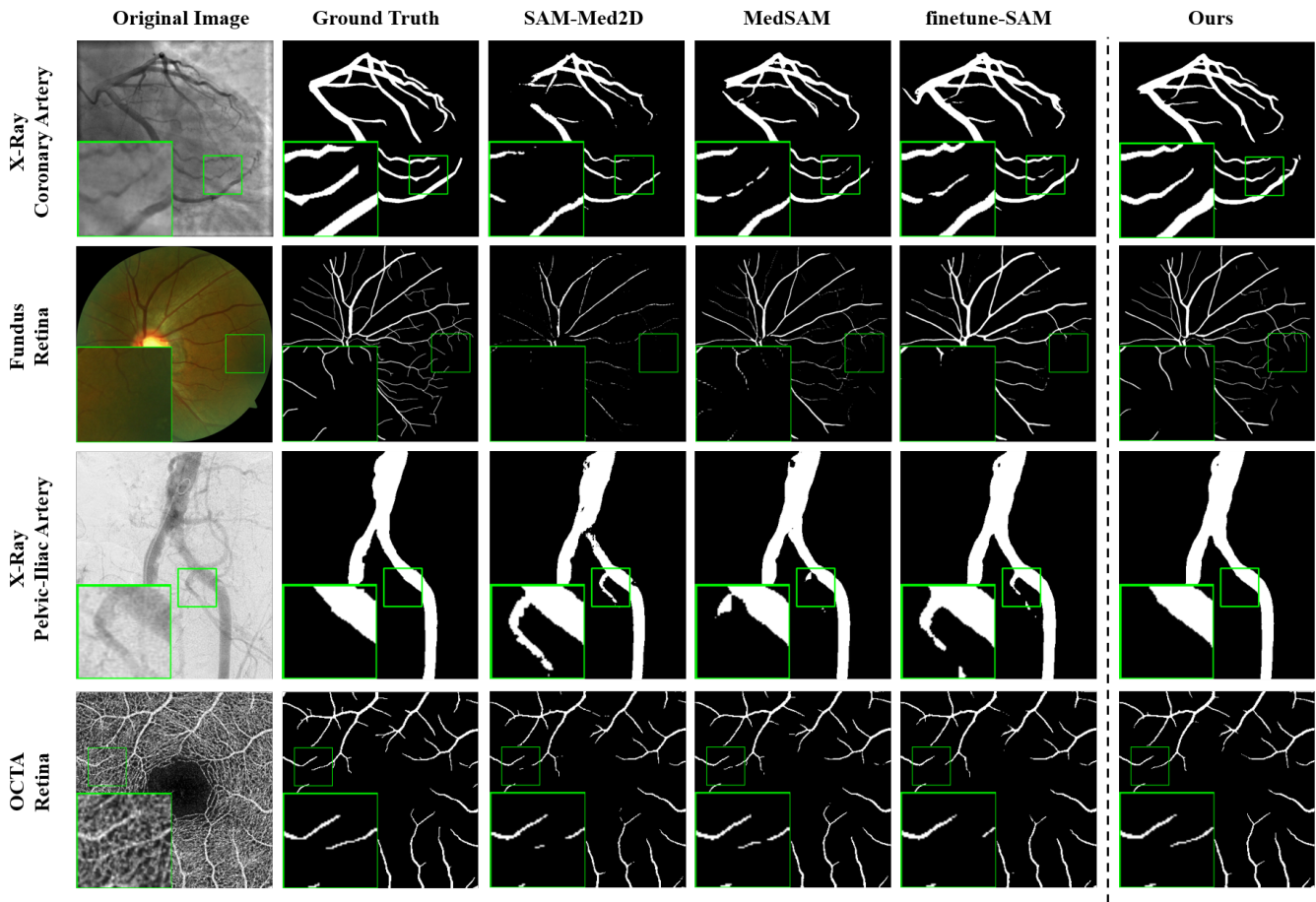


Fig. 3. Comparison with other SAM-based methods. From top to bottom, the images are from XCAD, ORVS, DrSAM and OCTA500-3M datasets. Due to the micro vessel enhancement module and the post-processing network, our method is better able to handle detailed information, resulting in superior performance in processing micro-vessels and maintaining vessel connectivity compared to other methods.

vascular structures, improving its segmentation performance across varying vessel sizes and shapes.

E. Morphological Correction based Post-Process Network

Unlike typical segmentation tasks, vessel segmentation imposes stringent requirements on the connectivity of the segmentation results. This connectivity is essential for accurate hemodynamic analysis, which aids in assessing patient health and prognosis, ultimately improving healthcare outcomes. To meet these requirements, we introduce a post-processing network based on morphological correction. The principle is inspired by Masked Image Modeling (MIM), but instead of masking random regions, we mask the fragmented areas of the vascular masks.

Given a network with both fragmented predicted masks and ground truth masks, the network is trained to predict the missing (i.e., fragmented) vascular structures. This allows the model to learn the correct connections at points of disconnection and repair the broken vessels. Simultaneously, for vessels that are meant to remain disconnected, the network ensures that these discontinuities are preserved. The post-processing is performed using a simple U-Net architecture, with MSE loss and CIDice loss [12] as the loss functions. By training on a

dataset that includes fragmented examples, even a basic U-Net model can learn to effectively repair disconnected vessels.

IV. EXPERIMENT

1) *Dataset*: To train a generalizable vessel segmentation model and assess its generalization capability, we constructed the largest vessel segmentation dataset, comprising 17 publicly available or request-access datasets. These datasets cover four types of images: X-ray Coronary Artery, Fundus Retina, OCTA Retina, and X-ray Pelvic Iliac Artery. Specifically, the coronary artery dataset includes 134XCA [38] (also known as DCA1) and XCAD [39]; the fundus dataset includes ARIA [40], CHASE_DB1 [41], DR-HAGIS [42], DRIVE [43], FIVES [44], HRF [45], IOSTAR [46], Les-AV [47], ORVS [48], and STARE [49]; the OCTA dataset includes ROSE-1 [18], ROSSA [50], and OCTA500 [51], with 39 pixel-level annotated images selected from ROSE-1; and the Pelvic-Iliac artery dataset is DrSAM [52].

We used 15 of these datasets for training and internal validation, each containing separate training, validation, and test sets. In addition, we evaluated the out-of-domain generalization of our model using the test sets from two additional datasets as external validation. Detailed information on the datasets is

TABLE I
DETAILS OF DATASETS USED IN OUR EXPERIMENTS

Dataset	Modality	Resolution	Train	Val	Test
ARIA	Fundus	768×576	108	12	43
CHASE_DB1	Fundus	960×999	18	2	8
DCA1(134XCA)	X-Ray	300×300	90	10	34
DR-HAGIS	Fundus	4752×3168	18	2	20
DRIVE	Fundus	584×565	18	2	20
DrSAM	X-Ray	386×448	360	40	100
FIVE	Fundus	2048×2048	540	60	200
Les-AV	Fundus	1620×1444	18	2	2
OCTA500-3M	OCTA	304×304	135	15	50
OCTA500-6M	OCTA	400×400	180	20	100
ORVS	Fundus	1444×1444	38	4	7
ROSE-1	OCTA	304×304	27	3	9
ROSSA	OCTA	320×320	736	82	100
STARE	Fundus	605×700	14	2	4
XCAD	X-Ray	512×512	75	9	42
HRF	Fundus	3504×2336	\	\	15
IOSTAR	Fundus	1024×1024	\	\	10

provided in Tables I. During training, all input images were resized to 1024×1024 and intensity normalization was applied.

A. Experimental Setup

We used the SAM model with a ViT-B architecture as the backbone, loading the corresponding pre-trained weights. In the macro vessel extraction module, we froze the ViT parameters during training, allowing only the adapters to be trained. The network and training were implemented in PyTorch on a Tesla V100-PCIE-32GB GPU. The principal segmentation network, as the initial module in our framework, was trained for 20 epochs with a batch size of 2, a learning rate of 0.001, and the AdamW optimizer. We used a combination of binary cross-entropy and Dice loss to improve vessel detection accuracy. The post-processing network, following the primary segmentation, was trained for 5 epochs with the same batch size, learning rate, and optimizer. Here, we applied Mean Squared Error (MSE) and CIDice loss to refine the segmentation results, ensuring more precise vessel delineation.

For evaluation metrics, we selected Dice and Intersection over Union (IoU) to assess the overall segmentation performance. Additionally, recognizing that improvements in connectivity may not significantly affect pixel-based metrics such as Dice, we introduced additional metrics to evaluate the connectivity of the segmentation results: CIDice and the normalized Betti number β_0 . The normalized Betti number β_0 is calculated as follows:

$$\beta_0 = \frac{1}{N} \sum_{i=1}^N |CC(X_i) - CC(Y_i)|$$

Which, referring to the methodology above, we split a mask into multiple 64×64 patches, where N represents the number of patches and CC denotes the number of disconnected components within a patch.

B. Comparing with SAM Based Method

In this section, we validate the performance of our proposed method by comparing OVS-Net with several state-of-the-art SAM-based segmentation networks, including MedSAM [21], MSA [23], SAM-Med2D [22], Finetune-SAM [53], SAM-UNet [54], and HQ-SAM [28], on both internal and external validation datasets. To ensure a fair comparison, we trained these SAM methods on the constructed vessel dataset, adhering to their respective default training protocols. The performance scores for different anatomical locations and modalities on both the internal and external validation datasets are presented in Table II. Thanks to its multi-scale vessel extraction capability and morphological correction-based post-processing network, OVS-Net outperformed the other methods, achieving the highest average Dice, IoU, and CIDice scores, along with the lowest β_0 score. Compared to the second-best SAM method, OVS-Net improved the average Dice score by 1.46 and improved connectivity by 34.6%. Figure 3 visualizes the segmentation results across various datasets, showing that our method effectively captures small vessels and addresses vessel discontinuities. Figure 4 further visualizes the radar chart comparing OVS-Net and the suboptimal SAM method on datasets with complex vascular structures, highlighting our method’s superior performance on high-resolution datasets with intricate and fine vessels (e.g., Dr-Hagis, ORVS, HRF). This demonstrates the effectiveness of OVS-Net in handling small vessel segmentation, which is crucial for clinical applications where precise vessel delineation impacts diagnostic and therapeutic decisions. Furthermore, OVS-Net maintained its competitive edge on the external dataset, achieving the best performance with a 1.79 improvement in average Dice scores and a 30.7% improvement in connectivity. These results not only demonstrate the effectiveness of OVS-Net but also highlight its strong generalization ability across diverse datasets and imaging modalities, underscoring its potential for broader clinical applications.

C. Comparing with Task-Specific Expert Methods

In this section, we present a comprehensive quantitative comparison of our method against various expert models on both internal and external validation datasets, providing a clear perspective on its performance relative to established benchmarks. The score comparisons for representative datasets are shown in Tables III, IV, and V, while external validation dataset scores are provided in Table VI. The scores of expert models are taken from [55], [56], [57], [58], [59], and [46], with [57] being the only source reporting standard deviation. We also plotted a bar chart in Figure 5 to compare the scores of OVS-Net with the expert models. For the expert model selection, we chose the model with the highest Dice score for comparison.

In Table III, we compare the segmentation scores of our method with 11 prominent expert models, including U-Net [60], U-Net++ [61], Attention-Unet [62], CE-Net [63], CAU-Net [64], CS²-Net [65], FR-Net [16], DE-DCGCN-EE [66], GT-DLA-dsHFF [67], and SPIRONet [55], across two coronary artery datasets. Our method outperforms all others in

TABLE II

COMPARED WITH SAM-BASED METHODS, WE REPORT THE INDIVIDUAL SCORES FOR CORONARY ARTERY, FUNDUS, OCTA, AND PELVIC-ILIAC ARTERY IN THE INTERNAL VALIDATION DATASET, AS WELL AS THE SCORES IN THE EXTERNAL VALIDATION DATASET. THE BEST SCORES ARE IN BOLD, AND THE SECOND-BEST METHODS ARE UNDERLINED; THE SAME APPLIES BELOW.

Method	Xray-Coronary_Artery				Fundus-Retina			
	Dice \uparrow	IoU \uparrow	clDice \uparrow	$\beta_0\downarrow$	Dice \uparrow	IoU \uparrow	clDice \uparrow	$\beta_0\downarrow$
MedSAM [21]	80.40 \pm 3.78	67.38 \pm 5.28	86.59 \pm 4.04	0.26 \pm 0.12	82.57 \pm 9.55	71.30 \pm 12.24	82.97 \pm 10.52	0.33 \pm 0.39
MSA [23]	74.60 \pm 3.24	59.60 \pm 4.09	81.44 \pm 4.80	0.52 \pm 0.25	71.72 \pm 8.58	56.49 \pm 8.92	71.24 \pm 9.44	0.44 \pm 0.49
SAM-Med2D [22]	75.74 \pm 6.02	61.32 \pm 7.72	80.41 \pm 6.94	0.50 \pm 0.27	78.43 \pm 12.66	66.02 \pm 14.67	78.98 \pm 13.36	0.35 \pm 0.38
Finetune-SAM [53]	78.44 \pm 4.48	64.75 \pm 6.07	84.22 \pm 5.21	0.31 \pm 0.13	79.13 \pm 9.78	66.37 \pm 11.38	77.61 \pm 11.04	0.37 \pm 0.43
SAM-UNet [54]	67.09 \pm 22.82	43.11 \pm 19.99	61.61 \pm 23.63	0.55 \pm 0.36	79.33 \pm 13.39	67.36 \pm 14.49	79.61 \pm 14.55	0.28 \pm 0.29
HQ-SAM [28]	76.61 \pm 4.30	62.28 \pm 5.63	80.42 \pm 5.45	0.77 \pm 0.45	77.37 \pm 10.70	64.15 \pm 12.40	77.40 \pm 11.08	0.39 \pm 0.31
OVS-Net	81.67\pm3.50	69.17\pm5.03	87.37\pm4.12	0.20\pm0.09	85.06\pm8.51	74.83\pm11.35	87.07\pm8.85	0.18\pm0.20
Method	OCTA-Retina				Xray-Pelvic_Iliac_Artery			
	Dice \uparrow	IoU \uparrow	clDice \uparrow	$\beta_0\downarrow$	Dice \uparrow	IoU \uparrow	clDice \uparrow	$\beta_0\downarrow$
MedSAM [21]	89.58 \pm 3.19	81.28 \pm 5.07	91.45 \pm 3.27	0.98 \pm 0.38	96.62 \pm 1.64	93.51 \pm 2.97	97.56 \pm 2.59	0.05 \pm 0.05
MSA [23]	80.35 \pm 6.32	67.59 \pm 8.41	83.14 \pm 6.32	1.68 \pm 0.57	94.88 \pm 2.33	90.35 \pm 4.09	96.14 \pm 3.96	0.10 \pm 0.08
SAM-Med2D [22]	84.99 \pm 3.73	74.08 \pm 5.49	87.50 \pm 4.16	1.70 \pm 0.54	95.14 \pm 2.23	90.82 \pm 3.92	96.40 \pm 3.30	0.11 \pm 0.08
Finetune-SAM [53]	87.41 \pm 3.72	77.81 \pm 5.61	89.39 \pm 4.00	1.20 \pm 0.42	96.31 \pm 1.85	92.94 \pm 3.33	97.31 \pm 2.82	0.05 \pm 0.42
SAM-UNet [54]	88.25 \pm 3.97	79.19 \pm 6.12	90.49 \pm 3.98	1.05 \pm 0.37	80.95 \pm 19.25	71.66 \pm 22.97	82.22 \pm 18.71	0.21 \pm 0.17
HQ-SAM [28]	86.76 \pm 4.53	76.82 \pm 6.47	88.72 \pm 4.76	1.93 \pm 0.57	95.10 \pm 2.26	90.73 \pm 3.98	93.84 \pm 4.89	0.2861 \pm 0.24
OVS-Net	90.36\pm3.21	82.57\pm5.18	92.20\pm3.08	0.67\pm0.30	96.64\pm1.90	93.56\pm3.43	97.57\pm2.94	0.05\pm0.61
Method	External Validation Dataset				Average			
	Dice \uparrow	IoU \uparrow	clDice \uparrow	$\beta_0\downarrow$	Dice \uparrow	IoU \uparrow	clDice \uparrow	$\beta_0\downarrow$
MedSAM [21]	74.83 \pm 3.29	59.89 \pm 4.24	73.16 \pm 6.25	0.40 \pm 0.14	86.61 \pm 8.47	77.28 \pm 12.03	88.06 \pm 9.18	0.52 \pm 0.49
MSA [23]	71.07 \pm 3.51	55.24 \pm 4.09	63.85 \pm 4.96	0.47 \pm 0.15	78.22 \pm 10.20	65.35 \pm 13.59	79.57 \pm 11.44	0.85 \pm 0.79
SAM-Med2D [22]	69.50 \pm 7.59	53.73 \pm 8.28	68.54 \pm 6.87	0.55 \pm 0.38	82.60 \pm 10.61	71.57 \pm 13.69	84.25 \pm 11.24	0.82 \pm 0.79
Finetune-SAM [53]	71.76 \pm 3.34	56.06 \pm 4.14	68.69 \pm 5.57	0.43 \pm 0.14	84.19 \pm 9.27	73.69 \pm 12.68	84.84 \pm 10.70	0.63 \pm 0.58
SAM-UNet [54]	73.40 \pm 4.34	58.17 \pm 5.50	72.92 \pm 7.82	0.39 \pm 0.10	80.73 \pm 15.48	69.91 \pm 17.45	82.18 \pm 15.81	0.57 \pm 0.48
HQ-SAM [28]	70.47 \pm 4.86	54.63 \pm 5.87	73.35 \pm 4.50	0.57 \pm 0.43	82.91 \pm 10.03	71.94 \pm 13.36	83.86 \pm 10.26	0.97 \pm 0.85
OVS-Net	77.62\pm3.95	63.60\pm5.32	78.93\pm5.80	0.27\pm0.05	88.05\pm7.49	79.38\pm10.95	90.14\pm7.40	0.34\pm0.33

TABLE III

QUANTITATIVE COMPARISON OF OUR OVS-NET AND SOTA TASK-SPECIFIC EXPERT METHODS ON CORONARY ARTERY SEGMENTATION TASK

Method	DCAI(134XCA)		XCAD	
	Dice	IoU	Dice	IoU
U-Net [60]	78.90	65.31	80.74	67.98
U-Net++ [61]	78.45	64.69	80.43	67.56
Attention-Unet [62]	78.04	64.18	79.98	66.94
CE-Net [63]	77.84	63.87	79.95	66.8
CAU-Net [64]	77.82	63.88	79.31	66.06
TransUNet [68]	78.82	65.19	80.24	67.28
CS ² -Net [65]	77.87	63.94	79.23	65.98
FR-UNet [20]	79.59	66.22	79.79	66.66
DE-DCGCN-EE [66]	77.82	63.87	79.12	65.76
GT-DLA-dsHFF [67]	77.17	62.97	80.44	67.53
SPIRONet [55]	79.75	66.45	81.76	69.73
OVS-Net	80.55	67.57	83.14	71.25
	\pm 3.46	\pm 4.88	\pm 2.98	\pm 4.43

coronary artery segmentation, achieving average Dice scores of 80.55 and 83.14, surpassing the latest state-of-the-art methods. This notable improvement underscores the effectiveness of our model in accurately delineating vascular structures, which is crucial for clinical decision-making in cardiovascular health.

For retinal fundus datasets, Table IV compares our approach with five expert models: U-Net [60], U-Net++ [61], Attention-UNet [62], CS-Net [69], and H2Former [70] across three datasets. On all three fundus datasets, our method consistently

TABLE IV

QUANTITATIVE COMPARISON OF OUR OVS-NET AND SOTA TASK-SPECIFIC EXPERT METHODS ON FUNDUS SEGMENTATION TASK

Method	DRIVE		STARE		CHASE_DB1	
	Dice	IoU	Dice	IoU	Dice	IoU
U-Net [60]	81.41	68.64	81.18	68.56	78.98	65.26
U-Net++ [61]	81.14	68.27	81.50	69.02	80.15	66.88
Attention-Unet [62]	80.39	67.21	81.06	68.39	79.64	66.17
CS-Net [69]	80.39	70.17	81.59	69.12	80.42	67.25
H2Former [70]	74.54	59.71	77.56	63.42	74.92	59.98
OVS-Net	81.93	69.43	82.54	70.27	81.36	68.61
	\pm 1.55	\pm 2.25	\pm 0.50	\pm 0.73	\pm 1.61	\pm 2.28

achieves the highest average Dice and IoU scores, demonstrating its robustness in handling variations in retinal images. While OVS-Net achieves the highest Dice score on the DRIVE dataset, it records a slightly lower IoU compared to CS-Net.

TABLE V

QUANTITATIVE COMPARISON OF OUR OVS-NET AND SOTA TASK-SPECIFIC EXPERT METHODS ON OCTA SEGMENTATION TASK

Method	OCTA500-3M		OCTA500-6M	
	Dice	IoU	Dice	IoU
U-Net [60]	90.60 \pm 2.16	82.88 \pm 3.47	88.28 \pm 2.59	79.11 \pm 3.97
MFI-Net [71]	90.15 \pm 1.59	82.15 \pm 2.57	88.62 \pm 2.57	79.59 \pm 3.77
Swin-Unet [72]	84.42 \pm 2.87	73.14 \pm 4.19	82.40 \pm 2.68	70.16 \pm 3.78
H2Former [70]	83.82 \pm 1.86	72.24 \pm 3.22	82.45 \pm 2.57	70.25 \pm 3.74
OVS-Net	91.32\pm2.10	84.10\pm3.38	88.68\pm2.28	79.74\pm3.55

TABLE VI
QUANTITATIVE SCORE COMPARISON WITH EXPERT MODELS ON TWO EXTERNAL VALIDATION DATASETS

Method	HRF	Method	IOSTAR
U-Net [60]	72.39	U-Net [60]	76.96
CS-Net [69]	71.04	DNN [73]	76.01
SA-UNet [74]	71.18	R2UNet [75]	77.16
SCS-Net [13]	70.66	Symmetry Filter [76]	74.31
CogSeg [77]	74.75	VA-UFL [78]	73.99
SuperVessel [79]	76.74	MSR-Net [80]	76.17
BioNet [59]	76.26	SUD-GAN [81]	76.96
OVS-Net	77.14 ± 4.05	OVS-Net	78.82 ± 3.43

TABLE VII
COMPARISON OF CONNECTIVITY-BASED POST-PROCESSING METHODS. WE CONDUCTED A COMPARISON OF OUR METHOD WITH CONNECTIVITY-FOCUSED POST-PROCESSING APPROACHES ON THE DRIVE, CHASE_DB1, AND DCA1 DATASETS.

Method	DRIVE		CHASE_DB1		DCA1	
	cDice	β_0	cDice	β_0	cDice	β_0
UNet [60]	81.9 \pm 4.0	0.79 \pm 0.16	84.1 \pm 2.6	0.40 \pm 0.13	84.5 \pm 4.6	0.36 \pm 0.17
ErrorNet [82]	81.6 \pm 3.9	0.85 \pm 0.18	83.7 \pm 2.7	0.41 \pm 0.10	85.5 \pm 4.5	0.27 \pm 0.13
TopoLoss [83]	81.9 \pm 3.8	0.77 \pm 0.14	84.4 \pm 2.5	0.40 \pm 0.06	84.9 \pm 4.8	0.28 \pm 0.11
LIOT [84]	81.5 \pm 4.3	0.80 \pm 0.16	83.9 \pm 2.7	0.41 \pm 0.12	85.1 \pm 4.4	0.33 \pm 0.12
DconnNet [85]	81.5 \pm 4.3	0.80 \pm 0.16	83.9 \pm 2.7	0.41 \pm 0.12	85.1 \pm 4.4	0.33 \pm 0.12
OVS-Net	82.1\pm3.90	0.61\pm0.13	84.4\pm2.3	0.26\pm0.03	87.4\pm4.4	0.22\pm0.11

Table V presents a detailed comparison of our method on two retinal OCTA datasets against 4 expert models, including U-Net [60], MFI-Net [71], Swin-Unet [72] and H2Former [70]. Our method achieves the highest Dice and IoU scores on the OCTA500-3M and OCTA500-6M dataset, showcasing its effectiveness in segmenting intricate vascular patterns typical in OCTA images further affirming our model’s versatility and capability to perform comparably to, or even surpass, expert models across multiple tasks.

In Table VI, we present a comparison of Dice scores of OVS-Net on two external validation datasets, HRF and IOSTAR, compared to 13 expert models, including U-Net [60], CS-Net [69], SAUNet [74], SCS-Net [13], CogSeg [77], SuperVessel [79], BioNet [59], DNN [73], R2UNet [75], Symmetry Filter [76], VA-UFL [78], MSR-Net [80], and SUD-GAN [81]. Our method achieved the highest scores on both datasets, with an average Dice score of 77.14 on the HRF dataset and 79.19 on the IOSTAR dataset. This demonstrates the potential of our approach to address the limitations of task-specific expert models, showing its ability to effectively recognize vascular structures of varying scales across different data distribution scenarios. Such a capability is particularly valuable for clinical applications, as expert models often struggle to generalize across different imaging conditions or data variations. Additionally, they may require extensive retraining on data obtained from different imaging modalities, scanners, or protocols, leading to substantial operational costs.

Additionally, we provide a comparison of connectivity metrics with expert models in Table VII. This table reports connectivity performance on the DRIVE, CHASE, and DCA1 datasets against specific segmentation networks or loss func-

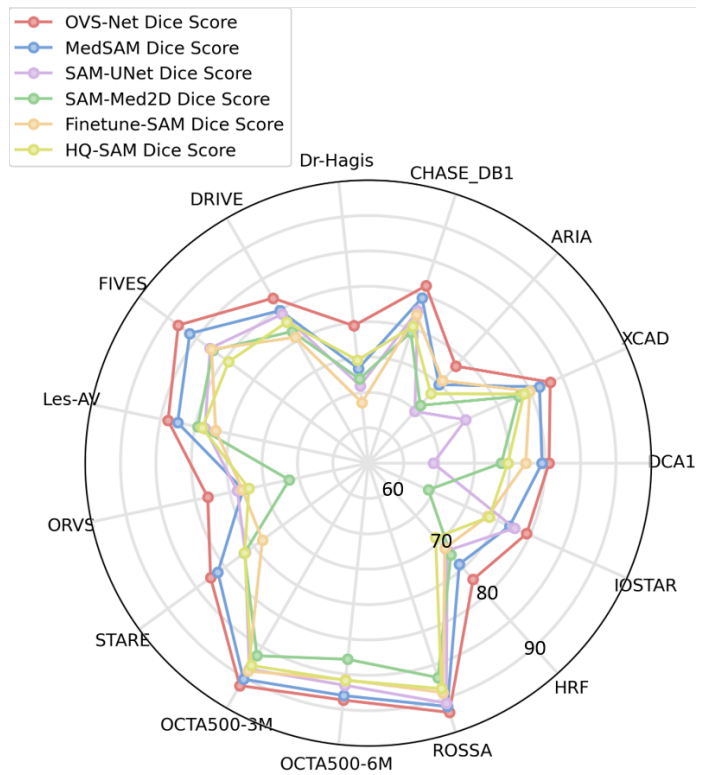


Fig. 4. Radar chart of scores on complex vascular datasets compared with the suboptimal SAM model.

TABLE VIII
QUANTITATIVE COMPARISON OF ABLATION STUDY FOR OVS-NET

Adapter	Micro Vessel Enhancement	Feature Connection	Post-processing	Dice	β_0
×	×	×	×	86.97	0.53
✓	×	×	×	87.21	0.53
✓	✓	×	×	88.24	0.49
✓	✓	✓	×	88.28	0.48
✓	✓	✓	✓	88.37	0.34

tions: Unet [60], ErrorNet [82], TopoLoss [83], LIOT [84], and DconnNet [85]. The expert model scores are reported from [31]. As shown in the table, our method, enhanced by a morphological correction-based post-processing network, achieves leading performance compared to specific expert models. This result is particularly notable, as it highlights our approach’s ability to not only deliver high-quality segmentation but also ensure that the segmented vessels maintain structural continuity—a crucial factor in clinical applications where accurate vascular connectivity is essential for diagnosis and treatment.

D. Ablation Study

To validate the effectiveness of the proposed improvements, we conducted a series of ablation studies on the internal validation dataset. In these experiments, we incrementally added the adapter, micro vessel enhancement module, feature concatenation in the Mask Decoder, and the morphological correction-based post-processing network to the baseline model. The Dice score and Betti number β_0 were used as

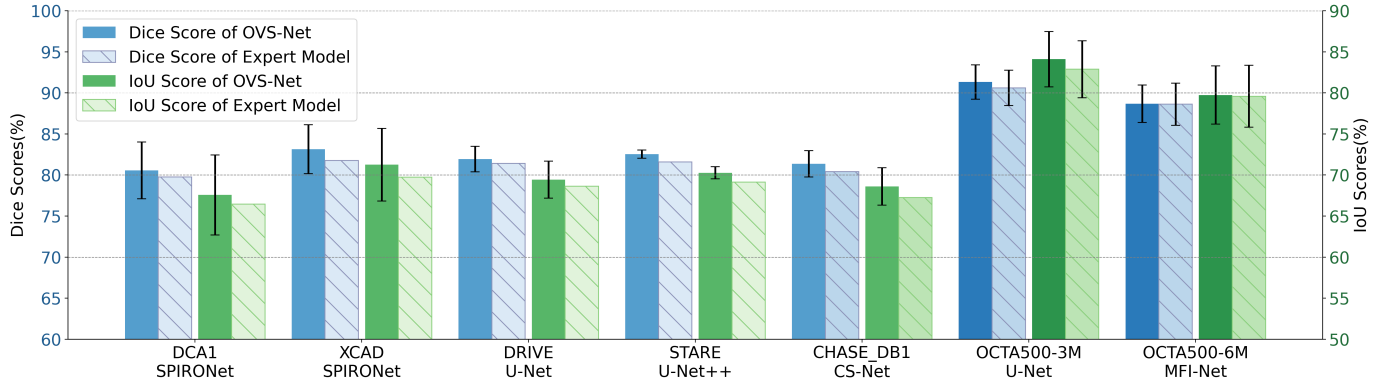


Fig. 5. Bar chart comparing the scores of OVS-Net and the expert model. Here we use the standard deviation as the error bar standard. For expert model selection, we select the expert model with the highest Dice score to plot the bar chart.

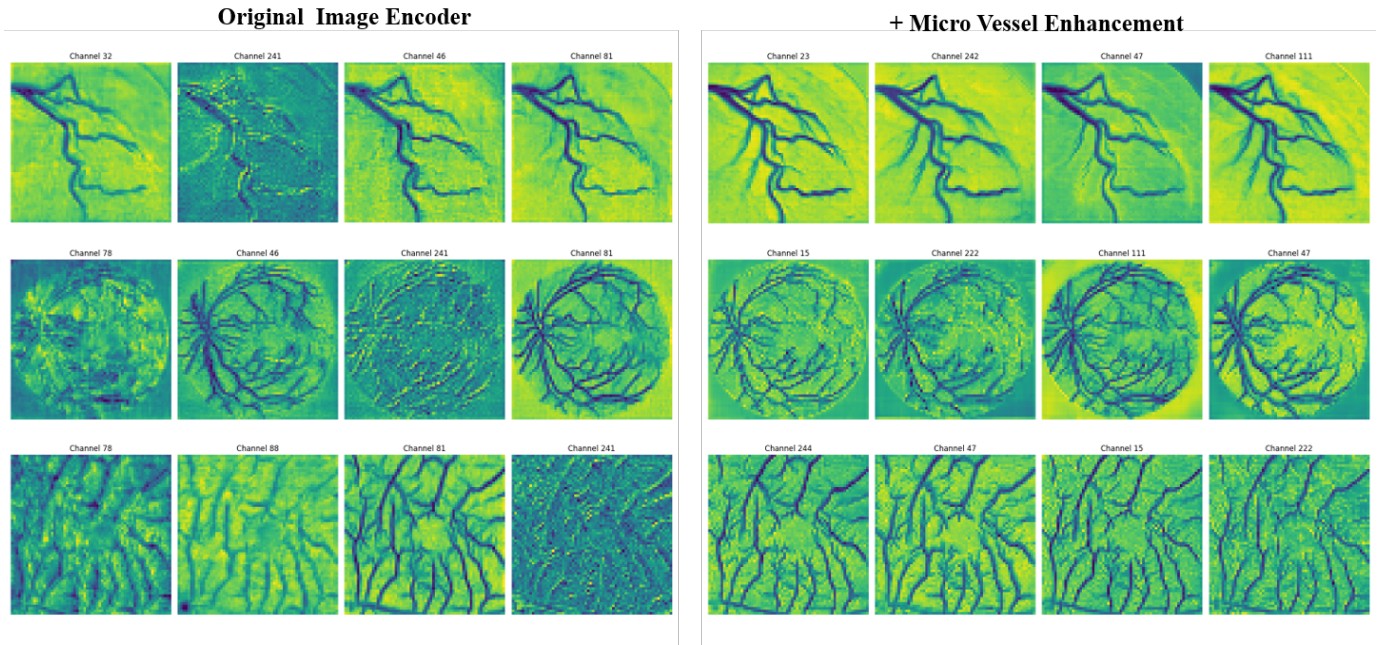


Fig. 6. Feature map visualization. We selected the four channels with the highest average activation values for visualization. The feature maps after incorporating the micro vessel enhancement module show notable improvement in extracting vascular network features.

performance metrics, and the results for each configuration are reported in Table VIII. The experimental results show that each modification improves SAM’s performance on vascular imaging, with the micro vessel enhancement module and post-processing network having the most significant impact on segmentation accuracy.

After integrating the micro vessel enhancement module, we observed a 1.31-point increase in the average Dice score, indicating a significant improvement in segmentation precision. To better illustrate this improvement, we visualized the feature activation maps before and after incorporating the module, as shown in Figure 6. In this visualization, we selected the four channels with the highest mean activation for closer examination. The feature maps show a clear enhancement in delineating vascular boundaries and a stronger focus on small vessel after the module was added. This suggests that the micro vessel enhancement module helps the network capture features

more effectively across different vessel sizes, which is crucial for accurate segmentation in complex vascular structures.

Furthermore, after incorporating the post-processing network, we observed a reduction of 0.14 in the Betti number β_0 , indicating improved connectivity in the segmentation results. To visually demonstrate this, Figure 7 compares the segmentation outcomes from the Primary Segmentation phase, before and after applying the post-processing network. In this figure, blue boxes highlight areas where the network successfully preserved inherent disconnections in the ground truth, while green boxes show where it effectively corrected segmentation breaks. Importantly, the post-processing network not only repairs these breaks but also preserves natural disconnections found in the original data, which is valuable for clinical applications as it ensures the segmented results align with the anatomical features of vascular structures.

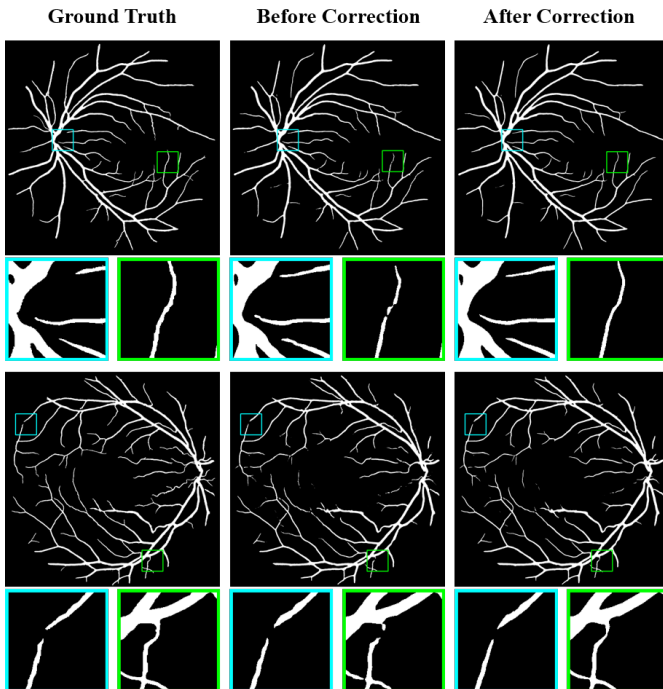


Fig. 7. Post-processing effect visualization. The blue boxes indicate preserved original discontinuities, while the green boxes represent vessels whose predicted discontinuities have been successfully repaired.

V. CONCLUSION

In this paper, we propose OVS-Net, a novel network exploring the Segment Anything Model (SAM) for optimized vessel segmentation. OVS-Net features five key modules: a macro vessel extraction module, micro vessel enhancement module, prompt encoder, mask prediction module, and a morphological correction-based post-processing network. The hybrid encoder architecture exploits SAM's Vision Transformer (ViT) for macro feature extraction with a convolution-based module for enhancing fine vessel structures and edges, critical for precise segmentation. Low-level feature fusion in the mask prediction module integrates global and local features, enabling accurate segmentation across varying scales and complexities. The post-processing network further improves clinical relevance by correcting vessel disconnections while preserving natural anatomical gaps, ensuring segmentation results are both accurate and meaningful.

Comprehensive experiments across 17 datasets demonstrate that OVS-Net achieves superior segmentation accuracy, enhanced connectivity, and robust generalization across diverse imaging modalities. While this study focuses on technical evaluation, future work will aim to integrate OVS-Net into clinical workflows, conducting user studies to assess its practical impact and potential to improve diagnostic and therapeutic outcomes, ultimately benefiting patient care.

REFERENCES

[1] G. Brugnara, M. Baumgartner, E. D. Scholze, K. Deike-Hofmann, K. Kades, J. Scherer, S. Denner, H. Meredig, A. Rastogi, M. A. Mahmutoglu *et al.*, "Deep-learning based detection of vessel occlusions on CT-angiography in patients with suspected acute ischemic stroke," *Nature Communications*, vol. 14, no. 1, p. 4938, 2023.

[2] S. Wang, C. Li, R. Wang, Z. Liu, M. Wang, H. Tan, Y. Wu, X. Liu, H. Sun, R. Yang *et al.*, "Annotation-efficient deep learning for automatic medical image segmentation," *Nature communications*, vol. 12, no. 1, p. 5915, 2021.

[3] S. Chaudhuri, S. Chatterjee, N. Katz, M. Nelson, and M. Goldbaum, "Detection of blood vessels in retinal images using two-dimensional matched filters," *IEEE Transactions on medical imaging*, vol. 8, no. 3, pp. 263–269, 1989.

[4] A. Hoover, V. Kouznetsova, and M. Goldbaum, "Locating blood vessels in retinal images by piecewise threshold probing of a matched filter response," *IEEE Transactions on Medical imaging*, vol. 19, no. 3, pp. 203–210, 2000.

[5] Z. Liu, Y. Lin, Y. Cao, H. Hu, Y. Wei, Z. Zhang, S. Lin, and B. Guo, "Swin transformer: Hierarchical vision transformer using shifted windows," in *Proceedings of the IEEE/CVF international conference on computer vision*, 2021, pp. 10 012–10 022.

[6] A. Krizhevsky, I. Sutskever, and G. E. Hinton, "ImageNet Classification with Deep Convolutional Neural Networks," *Advances in neural information processing systems*, vol. 25, 2012.

[7] X. Wang, G. Chen, G. Qian, P. Gao, X.-Y. Wei, Y. Wang, Y. Tian, and W. Gao, "Large-scale Multi-modal Pre-trained Models: A Comprehensive Survey," *Machine Intelligence Research*, vol. 20, no. 4, pp. 447–482, 2023.

[8] A. Kirillov, E. Mintun, N. Ravi, H. Mao, C. Rolland, L. Gustafson, T. Xiao, S. Whitehead, A. C. Berg, W.-Y. Lo *et al.*, "Segment Anything," in *Proceedings of the IEEE/CVF International Conference on Computer Vision*, 2023, pp. 4015–4026.

[9] Y. Huang, X. Yang, L. Liu, H. Zhou, A. Chang, X. Zhou, R. Chen, J. Yu, J. Chen, C. Chen *et al.*, "Segment Anything Model for Medical Images?" *Medical Image Analysis*, vol. 92, p. 103061, 2024.

[10] C. Chen, Q. Dou, H. Chen, J. Qin, and P.-A. Heng, "Synergistic image and feature adaptation: Towards cross-modality domain adaptation for medical image segmentation," in *Proceedings of the AAAI conference on artificial intelligence*, vol. 33, no. 01, 2019, pp. 865–872.

[11] R. J. Araújo, J. S. Cardoso, and H. P. Oliveira, "A Deep Learning Design for Improving Topology Coherence in Blood Vessel Segmentation," in *Medical Image Computing and Computer Assisted Intervention—MICCAI 2019: 22nd International Conference, Shenzhen, China, October 13–17, 2019, Proceedings, Part I 22*. Springer, 2019, pp. 93–101.

[12] S. Shit, J. C. Paetzold, A. Sekuboyina, I. Ezhov, A. Unger, A. Zhylyka, J. P. Pluim, U. Bauer, and B. H. Menze, "cDice – A Novel Topology-Preserving Loss Function for Tubular Structure Segmentation," in *Proceedings of the IEEE/CVF conference on computer vision and pattern recognition*, 2021, pp. 16 560–16 569.

[13] H. Wu, W. Wang, J. Zhong, B. Lei, Z. Wen, and J. Qin, "SCS-Net: A Scale and Context Sensitive Network for Retinal Vessel Segmentation," *Medical Image Analysis*, vol. 70, p. 102025, 2021.

[14] M. Jiang, Y. Zhu, and X. Zhang, "Covi-net: A hybrid convolutional and vision transformer neural network for retinal vessel segmentation," *Computers in Biology and Medicine*, vol. 170, p. 108047, 2024.

[15] N. Kang, M. Wang, C. Pang, R. Lan, B. Li, J. Guan, and H. Wang, "Cross-patch feature interactive net with edge refinement for retinal vessel segmentation," *Computers in Biology and Medicine*, vol. 174, p. 108443, 2024.

[16] H. Ning, C. Wang, X. Chen, and S. Li, "An Accurate and Efficient Neural Network for OCTA Vessel Segmentation and a New Dataset," in *ICASSP 2024-2024 IEEE International Conference on Acoustics, Speech and Signal Processing (ICASSP)*. IEEE, 2024, pp. 1966–1970.

[17] Z. Ma, D. Feng, J. Wang, and H. Ma, "Retinal OCTA Image Segmentation Based on Global Contrastive Learning," *Sensors*, vol. 22, no. 24, p. 9847, 2022.

[18] Y. Ma, H. Hao, J. Xie, H. Fu, J. Zhang, J. Yang, Z. Wang, J. Liu, Y. Zheng, and Y. Zhao, "Rose: A Retinal OCT-Angiography Vessel Segmentation Dataset and New Model," *IEEE transactions on medical imaging*, vol. 40, no. 3, pp. 928–939, 2020.

[19] S.-S. Chang, C.-T. Lin, W.-C. Wang, K.-C. Hsu, Y.-L. Wu, C.-H. Liu, and Y. C. Fann, "Optimizing ensemble U-Net architectures for robust coronary vessel segmentation in angiographic images," *Scientific Reports*, vol. 14, no. 1, p. 6640, 2024.

[20] W. Liu, H. Yang, T. Tian, Z. Cao, X. Pan, W. Xu, Y. Jin, and F. Gao, "Full-Resolution Network and Dual-Threshold Iteration for Retinal Vessel and Coronary Angiograph Segmentation," *IEEE journal of biomedical and health informatics*, vol. 26, no. 9, pp. 4623–4634, 2022.

[21] J. Ma, Y. He, F. Li, L. Han, C. You, and B. Wang, "Segment anything in medical images," *Nature Communications*, vol. 15, no. 1, p. 654, 2024.

- [22] J. Cheng, J. Ye, Z. Deng, J. Chen, T. Li, H. Wang, Y. Su, Z. Huang, J. Chen, L. Jiang *et al.*, "SAM-Med2D," *arXiv preprint arXiv:2308.16184*, 2023.
- [23] J. Wu, W. Ji, Y. Liu, H. Fu, M. Xu, Y. Xu, and Y. Jin, "Medical SAM Adapter: Adapting Segment Anything Model for Medical Image Segmentation," *arXiv preprint arXiv:2304.12620*, 2023.
- [24] K. Zhang and D. Liu, "Customized Segment Anything Model for Medical Image Segmentation," *arXiv preprint arXiv:2304.13785*, 2023.
- [25] S. Chai, R. K. Jain, S. Teng, J. Liu, Y. Li, T. Tateyama, and Y.-w. Chen, "Ladder fine-tuning approach for SAM integrating complementary network," *arXiv preprint arXiv:2306.12737*, 2023.
- [26] X. Lin, Y. Xiang, L. Zhang, X. Yang, Z. Yan, and L. Yu, "SAMUS: Adapting Segment Anything Model for Clinically-Friendly and Generalizable Ultrasound Image Segmentation," *arXiv preprint arXiv:2309.06824*, 2023.
- [27] C. Qin, J. Cao, H. Fu, and F. S. Kha, "DB-SAM: Delving into High Quality Universal Medical Image Segmentation," *arXiv preprint arXiv:2410.04172*, 2024.
- [28] L. Ke, M. Ye, M. Danelljan, Y.-W. Tai, C.-K. Tang, F. Yu *et al.*, "Segment Anything in High Quality," *Advances in Neural Information Processing Systems*, vol. 36, 2024.
- [29] H. Yuan, X. Li, L. Qi, T. Zhang, M.-H. Yang, S. Yan, and C. C. Loy, "Mamba or RWKV: Exploring High-Quality and High-Efficiency Segment Anything Model haobo yuan, xil," *arXiv preprint arXiv:2406.19369*, 2024.
- [30] Y. Qiu, Z. Li, Y. Wang, P. Dong, D. Wu, X. Yang, Q. Hong, and D. Shen, "CorSegRec: A Topology-Preserving Scheme for Extracting Fully-Connected Coronary Arteries from CT Angiography," in *International Conference on Medical Image Computing and Computer-Assisted Intervention*. Springer, 2023, pp. 670–680.
- [31] Q. Wu, Y. Chen, W. Liu, X. Yue, and X. Zhuang, "Deep Closing: Enhancing Topological Connectivity in Medical Tubular Segmentation," *IEEE Transactions on Medical Imaging*, 2024.
- [32] M. T. Teichmann and R. Cipolla, "Convolutional CRFs for Semantic Segmentation," *arXiv preprint arXiv:1805.04777*, 2018.
- [33] D. Jha, M. A. Riegler, D. Johansen, P. Halvorsen, and H. D. Johansen, "DoubleU-Net: A Deep Convolutional Neural Network for Medical Image Segmentation," in *2020 IEEE 33rd International symposium on computer-based medical systems (CBMS)*. IEEE, 2020, pp. 558–564.
- [34] H. Ye, X. Zhang, Y. Hu, H. Fu, and J. Liu, "VSR-Net: Vessel-like Structure Rehabilitation Network with Graph Clustering," *arXiv preprint arXiv:2312.13116*, 2023.
- [35] M. Wang, H. Ding, J. H. Liew, J. Liu, Y. Zhao, and Y. Wei, "SegRefiner: Towards Model-Agnostic Segmentation Refinement with Discrete Diffusion Process," *Advances in Neural Information Processing Systems*, vol. 36, pp. 79761–79780, 2023.
- [36] K. He, X. Chen, S. Xie, Y. Li, P. Dollár, and R. Girshick, "Masked Autoencoders Are Scalable Vision Learners," in *Proceedings of the IEEE/CVF conference on computer vision and pattern recognition*, 2022, pp. 16000–16009.
- [37] Z. Liu, H. Mao, C.-Y. Wu, C. Feichtenhofer, T. Darrell, and S. Xie, "A ConvNet for the 2020s," in *Proceedings of the IEEE/CVF conference on computer vision and pattern recognition*, 2022, pp. 11976–11986.
- [38] F. Cervantes-Sanchez, I. Cruz-Aceves, A. Hernandez-Aguirre, M. A. Hernandez-Gonzalez, and S. E. Solorio-Meza, "Automatic Segmentation of Coronary Arteries in X-ray Angiograms using Multiscale Analysis and Artificial Neural Networks," *Applied Sciences*, vol. 9, no. 24, p. 5507, 2019.
- [39] Y. Ma, Y. Hua, H. Deng, T. Song, H. Wang, Z. Xue, H. Cao, R. Ma, and H. Guan, "Self-Supervised Vessel Segmentation via Adversarial Learning," in *Proceedings of the IEEE/CVF International Conference on Computer Vision*, 2021, pp. 7536–7545.
- [40] D. J. Farnell, F. N. Hatfield, P. Knox, M. Reakes, S. Spencer, D. Parry, and S. P. Harding, "Enhancement of blood vessels in digital fundus photographs via the application of multiscale line operators," *Journal of the Franklin institute*, vol. 345, no. 7, pp. 748–765, 2008.
- [41] C. G. Owen, A. R. Rudnicka, R. Mullen, S. A. Barman, D. Monekosso, P. H. Whincup, J. Ng, and C. Paterson, "Measuring retinal vessel tortuosity in 10-year-old children: validation of the Computer-Assisted Image Analysis of the Retina (CAIAR) program," *Investigative ophthalmology & visual science*, vol. 50, no. 5, pp. 2004–2010, 2009.
- [42] S. Holm, G. Russell, V. Nourrit, and N. McLoughlin, "DR HAGIS—a fundus image database for the automatic extraction of retinal surface vessels from diabetic patients," *Journal of Medical Imaging*, vol. 4, no. 1, pp. 014503–014503, 2017.
- [43] J. Staal, M. D. Abramoff, M. Niemeijer, M. A. Viergever, and B. Van Ginneken, "Ridge-based vessel segmentation in color images of the retina," *IEEE transactions on medical imaging*, vol. 23, no. 4, pp. 501–509, 2004.
- [44] K. Jin, X. Huang, J. Zhou, Y. Li, Y. Yan, Y. Sun, Q. Zhang, Y. Wang, and J. Ye, "FIVES: A Fundus Image Dataset for Artificial Intelligence based Vessel Segmentation," *Scientific data*, vol. 9, no. 1, p. 475, 2022.
- [45] J. Odstrcilik, R. Kolar, A. Budai, J. Hornegger, J. Jan, J. Gazarek, T. Kubena, P. Cernosek, O. Svoboda, and E. Angelopoulou, "Retinal vessel segmentation by improved matched filtering: evaluation on a new high-resolution fundus image database," *IET Image Processing*, vol. 7, no. 4, pp. 373–383, 2013.
- [46] J. Zhang, B. Dashtbozorg, E. Bekkers, J. P. Pluim, R. Duits, and B. M. ter Haar Romeny, "Robust Retinal Vessel Segmentation via Locally Adaptive Derivative Frames in Orientation Scores," *IEEE transactions on medical imaging*, vol. 35, no. 12, pp. 2631–2644, 2016.
- [47] J. I. Orlando, J. Barbosa Breda, K. Van Keer, M. B. Blaschko, P. J. Blanco, and C. A. Bulant, "Towards a glaucoma risk index based on simulated hemodynamics from fundus images," in *Medical Image Computing and Computer Assisted Intervention—MICCAI 2018: 21st International Conference, Granada, Spain, September 16–20, 2018, Proceedings, Part II 11*. Springer, 2018, pp. 65–73.
- [48] A. Sarhan, J. Rokne, R. Alhaji, and A. Crichton, "Transfer Learning Through Weighted Loss Function and Group Normalization for Vessel Segmentation from Retinal Images," in *2020 25th International Conference on Pattern Recognition (ICPR)*. IEEE, 2021, pp. 9211–9218.
- [49] A. Hoover, V. Kouznetsova, and M. Goldbaum, "Locating blood vessels in retinal images by piecewise threshold probing of a matched filter response," *IEEE Transactions on Medical imaging*, vol. 19, no. 3, pp. 203–210, 2000.
- [50] H. Ning, C. Wang, X. Chen, and S. Li, "An Accurate and Efficient Neural Network for OCTA Vessel Segmentation and a New Dataset," in *ICASSP 2024-2024 IEEE International Conference on Acoustics, Speech and Signal Processing (ICASSP)*. IEEE, 2024, pp. 1966–1970.
- [51] M. Li, K. Huang, Q. Xu, J. Yang, Y. Zhang, Z. Ji, K. Xie, S. Yuan, Q. Liu, and Q. Chen, "OCTA-500: A Retinal Dataset for Optical Coherence Tomography Angiography Study," *Medical image analysis*, vol. 93, p. 103092, 2024.
- [52] V. Zohranyan, V. Navasardyan, H. Navasardyan, J. Borggreffe, and S. Navasardyan, "Dr-SAM: An End-to-End Framework for Vascular Segmentation Diameter Estimation and Anomaly Detection on Angiography Images," in *Proceedings of the IEEE/CVF Conference on Computer Vision and Pattern Recognition*, 2024, pp. 5113–5121.
- [53] H. Gu, H. Dong, J. Yang, and M. A. Mazurowski, "How to build the best medical image segmentation algorithm using foundation models: a comprehensive empirical study with Segment Anything Model," *arXiv preprint arXiv:2404.09957*, 2024.
- [54] S. Yang, H. Bi, H. Zhang, and J. Sun, "SAM-UNet: Enhancing Zero-Shot Segmentation of SAM for Universal medical images," *arXiv preprint arXiv:2408.09886*, 2024.
- [55] D.-X. Huang, X.-H. Zhou, X.-L. Xie, S.-Q. Liu, S.-Y. Wang, Z.-Q. Feng, M.-J. Gui, H. Li, T.-Y. Xiang, B.-X. Yao *et al.*, "SPIRONet: Spatial-Frequency Learning and Topological Channel Interaction Network for Vessel Segmentation," *arXiv preprint arXiv:2406.19749*, 2024.
- [56] W. Liu, H. Yang, T. Tian, Z. Cao, X. Pan, W. Xu, Y. Jin, and F. Gao, "Full-Resolution Network and Dual-Threshold Iteration for Retinal Vessel and Coronary Angiograph Segmentation," *IEEE journal of biomedical and health informatics*, vol. 26, no. 9, pp. 4623–4634, 2022.
- [57] X. Tan, X. Chen, Q. Meng, F. Shi, D. Xiang, Z. Chen, L. Pan, and W. Zhu, "OCT2Former: A retinal OCT-angiography vessel segmentation transformer," *Computer Methods and Programs in Biomedicine*, vol. 233, p. 107454, 2023.
- [58] T. M. Khan, M. Arsalan, S. Iqbal, I. Razzak, and E. Meijering, "Feature Enhancer Segmentation Network (FES-Net) for Vessel Segmentation," in *2023 International Conference on Digital Image Computing: Techniques and Applications (DICTA)*. IEEE, 2023, pp. 160–167.
- [59] M. Matloob Abbasi, S. Iqbal, K. Aurangzeb, M. Alhussein, and T. M. Khan, "LMBiS-Net: A lightweight bidirectional skip connection based multipath CNN for retinal blood vessel segmentation," *Scientific Reports*, vol. 14, no. 1, p. 15219, 2024.
- [60] O. Ronneberger, P. Fischer, and T. Brox, "U-net: Convolutional networks for biomedical image segmentation," in *Medical image computing and computer-assisted intervention—MICCAI 2015: 18th international conference, Munich, Germany, October 5–9, 2015, proceedings, part III 18*. Springer, 2015, pp. 234–241.
- [61] Z. Zhou, M. M. Rahman Siddiquee, N. Tajbakhsh, and J. Liang, "UNet++: A Nested U-Net Architecture for Medical Image Segmentation," in *Deep Learning in Medical Image Analysis and Multimodal*

- Learning for Clinical Decision Support: 4th International Workshop, DLMA 2018, and 8th International Workshop, ML-CDS 2018, Held in Conjunction with MICCAI 2018, Granada, Spain, September 20, 2018, Proceedings 4.* Springer, 2018, pp. 3–11.
- [62] O. Oktay, J. Schlemper, L. Le Folgoc, M. Lee, M. Heinrich, K. Misawa, K. Mori, S. McDonagh, N. Y. Hammerla, B. Kainz *et al.*, “Attention U-Net: Learning Where to Look for the Pancreas,” in *Medical Imaging with Deep Learning*.
- [63] Z. Gu, J. Cheng, H. Fu, K. Zhou, H. Hao, Y. Zhao, T. Zhang, S. Gao, and J. Liu, “CE-Net: Context Encoder Network for 2D Medical Image Segmentation,” *IEEE transactions on medical imaging*, vol. 38, no. 10, pp. 2281–2292, 2019.
- [64] R.-Q. Li, G.-B. Bian, X.-H. Zhou, X. Xie, Z.-L. Ni, and Z. Hou, “CAU-net: A Novel Convolutional Neural Network for Coronary Artery Segmentation in Digital Subtraction angiography,” in *Neural Information Processing: 27th International Conference, ICONIP 2020, Bangkok, Thailand, November 23–27, 2020, Proceedings, Part I 27.* Springer, 2020, pp. 185–196.
- [65] L. Mou, Y. Zhao, H. Fu, Y. Liu, J. Cheng, Y. Zheng, P. Su, J. Yang, L. Chen, A. F. Frangi *et al.*, “CS2-Net: Deep Learning Segmentation of Curvilinear Structures in Medical Imaging,” *Medical image analysis*, vol. 67, p. 101874, 2021.
- [66] Y. Li, Y. Zhang, W. Cui, B. Lei, X. Kuang, and T. Zhang, “Dual Encoder-Based Dynamic-Channel Graph Convolutional Network With Edge Enhancement for Retinal Vessel Segmentation,” *IEEE Transactions on Medical Imaging*, vol. 41, no. 8, pp. 1975–1989, 2022.
- [67] Y. Li, Y. Zhang, J.-Y. Liu, K. Wang, K. Zhang, G.-S. Zhang, X.-F. Liao, and G. Yang, “Global Transformer and Dual Local Attention Network via Deep-Shallow Hierarchical Feature Fusion for Retinal Vessel Segmentation,” *IEEE Transactions on Cybernetics*, vol. 53, no. 9, pp. 5826–5839, 2022.
- [68] J. Chen, Y. Lu, Q. Yu, X. Luo, E. Adeli, Y. Wang, L. Lu, A. L. Yuille, and Y. Zhou, “TransUNet: Transformers Make Strong Encoders for Medical Image Segmentation,” *arXiv preprint arXiv:2102.04306*, 2021.
- [69] L. Mou, Y. Zhao, L. Chen, J. Cheng, Z. Gu, H. Hao, H. Qi, Y. Zheng, A. Frangi, and J. Liu, “CS-Net: Channel and Spatial Attention Network for Curvilinear Structure Segmentation,” in *Medical Image Computing and Computer Assisted Intervention—MICCAI 2019: 22nd International Conference, Shenzhen, China, October 13–17, 2019, Proceedings, Part I 22.* Springer, 2019, pp. 721–730.
- [70] A. He, K. Wang, T. Li, C. Du, S. Xia, and H. Fu, “H2Former: An Efficient Hierarchical Hybrid Transformer for Medical Image Segmentation,” *IEEE Transactions on Medical Imaging*, vol. 42, no. 9, pp. 2763–2775, 2023.
- [71] Y. Ye, C. Pan, Y. Wu, S. Wang, and Y. Xia, “MFI-Net: Multiscale Feature Interaction Network for Retinal Vessel Segmentation,” *IEEE Journal of Biomedical and Health Informatics*, vol. 26, no. 9, pp. 4551–4562, 2022.
- [72] H. Cao, Y. Wang, J. Chen, D. Jiang, X. Zhang, Q. Tian, and M. Wang, “Swin-Unet: Unet-like Pure Transformer for Medical Image Segmentation,” in *European conference on computer vision*. Springer, 2022, pp. 205–218.
- [73] M. I. Meyer, P. Costa, A. Galdran, A. M. Mendonça, and A. Campilho, “A Deep Neural Network for Vessel Segmentation of Scanning Laser Ophthalmoscopy Images,” in *Image Analysis and Recognition: 14th International Conference, ICIAR 2017, Montreal, QC, Canada, July 5–7, 2017, Proceedings 14.* Springer, 2017, pp. 507–515.
- [74] C. Guo, M. Szemenyei, Y. Yi, W. Wang, B. Chen, and C. Fan, “SA-UNet: Spatial Attention U-Net for Retinal Vessel Segmentation,” in *2020 25th international conference on pattern recognition (ICPR)*. IEEE, 2021, pp. 1236–1242.
- [75] M. Z. Alom, M. Hasan, C. Yakopcic, T. M. Taha, and V. K. Asari, “Recurrent Residual Convolutional Neural Network based on U-Net (R2U-Net) for Medical Image Segmentation,” *arXiv preprint arXiv:1802.06955*, 2018.
- [76] Y. Zhao, Y. Zheng, Y. Liu, Y. Zhao, L. Luo, S. Yang, T. Na, Y. Wang, and J. Liu, “Automatic 2-D/3-D Vessel Enhancement in Multiple Modality Images Using a Weighted Symmetry Filter,” *IEEE transactions on medical imaging*, vol. 37, no. 2, pp. 438–450, 2017.
- [77] Q. Zhang, G. Yang, and G. Zhang, “Collaborative Network for Super-Resolution and Semantic Segmentation of Remote Sensing Images,” *IEEE Transactions on Geoscience and Remote Sensing*, vol. 60, pp. 1–12, 2021.
- [78] C. L. Srinidhi, P. Aparna, and J. Rajan, “A visual attention guided unsupervised feature learning for robust vessel delineation in retinal images,” *Biomedical Signal Processing and Control*, vol. 44, pp. 110–126, 2018.
- [79] Y. Hu, Z. Qiu, D. Zeng, L. Jiang, C. Lin, and J. Liu, “SuperVessel: Segmenting High-Resolution Vessel from Low-Resolution Retinal Image,” in *Chinese Conference on Pattern Recognition and Computer Vision (PRCV)*. Springer, 2022, pp. 178–190.
- [80] M. K. Kar, D. R. Neog, and M. K. Nath, “Retinal Vessel Segmentation Using Multi-Scale Residual Convolutional Neural Network (MSR-Net) Combined with Generative Adversarial Networks,” *Circuits, Systems, and Signal Processing*, vol. 42, no. 2, pp. 1206–1235, 2023.
- [81] T. Yang, T. Wu, L. Li, and C. Zhu, “SUD-GAN: Deep Convolution Generative Adversarial Network Combined with Short Connection and Dense Block for Retinal Vessel Segmentation,” *Journal of digital imaging*, vol. 33, pp. 946–957, 2020.
- [82] N. Tajbakhsh, B. Lai, S. P. Ananth, and X. Ding, “ErrorNet: Learning error representations from limited data to improve vascular segmentation,” in *2020 IEEE 17th International Symposium on Biomedical Imaging (ISBI)*. IEEE, 2020, pp. 1364–1368.
- [83] X. Hu, F. Li, D. Samaras, and C. Chen, “Topology-Preserving Deep Image Segmentation,” *Advances in neural information processing systems*, vol. 32, 2019.
- [84] T. Shi, N. Boutry, Y. Xu, and T. Géraud, “Local Intensity Order Transformation for Robust Curvilinear Object Segmentation,” *IEEE Transactions on Image Processing*, vol. 31, pp. 2557–2569, 2022.
- [85] Z. Yang and S. Farsiu, “Directional Connectivity-based Segmentation of Medical Images,” in *Proceedings of the IEEE/CVF conference on computer vision and pattern recognition*, 2023, pp. 11 525–11 535.